Experimental and theoretical evaluation of (*iso*)quinolinium bromide derivatives as corrosion inhibitors of steel E24 in 0.5 M H_2SO_4 solution

M.E. Said,[1,2] H. Allal,[1,3] B. Mezhoud,[1,4] M. Bouchouit,[1] A. Chibani[1] and A. Bouraiou[1]*

[1]Unité de Recherche de CHimie de l'Environnement, et Moléculaire Structurale, CHEMS, Université des Frères Mentouri, Constantine, Algeria
[2]Faculté de Technologie-BP 166 Université Mohamed Boudief M'sila 28000, Algeria
[3]Département Génie des Procédés, Faculté Génie des Procédés, Université Salah Boubnider Constantine 3, Constantine, Algeria
[4]Faculté des sciences Exactes et Informatique, Université Mouhamed Seddik Benyahial de Jijel BP 98 Ouled Aissa, Jijel 18000, Algeria
**E-mail: bouraiou.abdelmalek@umc.edu.dz*

Abstract

The ability of (2-methoxy-2-oxoethyl)quinolinium bromide (Qui^+, Br^-) and (2-methoxy-2-oxoethyl) iso quinolinium bromide (*iso*Qui^+, Br^-) were investigated for corrosion inhibition of mild steel E24 in H_2SO_4 by impedance spectroscopy and potentiodynamic polarization measurements. A series of experiments with various inhibitor concentrations were conducted. The results show that the corrosion rate decreases, inhibition efficiencies increase, and surface coverage increase with increasing inhibitor concentration. Potentiostatic polarization revealed that both inhibitors affected cathodic and anodic reactions, making them inhibitors of a mixed type with a significant cathodic inhibitory character. Several adsorption isotherms, including Langmuir, Temkin, and Frumkin, were investigated to understand the inhibitor's adsorption behaviour. The adsorption of both compounds on a mild steel surface obeys Langmuir's adsorption isotherm. In addition, the values of ΔG^0_{ads} showed a physisorption effect for the two prepared inhibitors. To compare the chemical reactivity of Qui^+, Br^- and *iso*Qui^+, Br^- and study the interactions between inhibitor molecules and the steel surface, different quantum chemical descriptors have been calculated, such as E_{HOMO}, E_{LUMO}, ΔE, χ, η, σ and ΔN. The results obtained reveal that the Qui^+, Br^- has higher electronegativity (χ), global softness (σ), and global electrophilicity (ω) than the *iso*Qui^+, Br^- compound. The order of *IE* determined from experimental measurements is successfully supported by theoretical analysis.

Received: May 22, 2023. Published June 8, 2023 doi: 10.17675/2305-6894-2023-12-2-16

Keywords: *corrosion inhibitors, steel corrosion, quinolinium salt, electrochemical measurements.*

1. Introduction

The usage of steel is well-pronounced in various industries, especially in manufacturing, oil, petroleum, construction, medical, textile, transport, and electrochemical industries. The corrosion mechanism of steel changes with the exposed media [1, 2]. In industry, acid solutions are widely used for many purposes, such as acid pickling, industrial acid cleaning, acid descaling, and oil well acidizing [3, 4]. The general aggressive nature of the acidic solution results in corrosive attacks. Therefore, it makes corrosion management investment projects in the metal industry hugely expensive. The strategies include using corrosion-resistant alloys or steel with corrosion inhibitors [5, 6]. The interaction between inhibitor molecules and the metal surface by adsorption of organic compounds inhibitors depends on several factors, such as the charge of the inhibitor and the nature of the metal surface, the structure of the inhibitors, the type of aggressive media, the extent of the aggressiveness, as well as the nature of its interaction with the metal surface [7, 8]. In general, effective corrosion inhibitors are organic compounds that contain heterogeneous atoms such as O, N, S, and P [9, 10]. Several works were conducted on organic salt compounds as corrosion inhibitors. The salt organic contains oxygen, sulfur, and nitrogen elements, which help in the corrosion inhibition process of various metals such as aluminium and steel in acid solutions with environmental considerations that have attracted more attention [11, 12]. The work is devoted to studying the inhibition characteristics of two compounds as inhibitors for steel E24 in H_2SO_4 solution, using potentiodynamic polarization measurements (Tafel) and electrochemical impedance spectroscopy (EIS). We calculated the Gibbs free energy (ΔG^0_{ads}) from experimental data of the inhibition process.

2. Experimental procedures

2.1. Preparation of corrosive solution

The studied corrosion solution is 0.5 M H_2SO_4 diluted from 98% concentrated acid with different concentrations of inhibitors.

2.2. Inhibitors

(2-Methoxy-2-oxoethyl)quinolinium bromide (Qui^+, Br^-) and (2-methoxy-2-oxoethyl) iso quinolinium bromide (*iso*Qui^+, Br^-) (Figure 1) were prepared by reaction of methyl 2-bromoacetate with quinoline or isoquinoline according to reported procedure [13, 14].

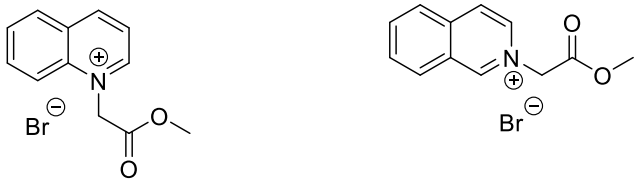

Figure 1. Structure of studied inhibitors.

2.3. Mild steel specimen

The working electrode is steel (E24) coated with epoxy resins and has an exposed area of 0.78 cm^2. The steel E24 has a chemical composition: C = 0.35%, Mn = 0.45%, S = 0.035%, P = 0.035%, Si = 0.25%, Cr = 1.7 and remainder Fe. We carried out measurements of galvanic and dynamic polarization on it.

The working electrode was polished with abrasive papers of different grades (150, 220, 400, 600, 1200, and 2000 grit), rinsed, degreased with ethanol, rinsed several times with distilled water, and dried before measurement.

A conventional three-electrode cylindrical glass cell was used for potentiodynamic polarization analysis and electrochemical impedance spectroscopy. Electrodes used for electrochemical measurements are a platinum counter electrode and a saturated calomel electrode as a reference electrode. Polarization and impedance measurements were done using a potentiostat/galvanostat/ZRA "GAMRY-Reference 3000". Potentiodynamic polarization experiments were performed in the potential range of –800 to –200 mV using a scan rate of 1 mV/s. Inhibition efficiency (*IE* %) values are obtained in this method using the following equation 1:

$$IE(\%) = \frac{I_{\text{corr(0)}} - I_{\text{corr(inh)}}}{I_{\text{corr(0)}}} \times 100 \quad (1)$$

where I_{corr} and $I_{\text{corr(0)}}$ are the current densities in the presence or absence of the investigated inhibitors, respectively.

Electrochemical impedance spectroscopy (EIS) was performed at open circuit potential (E_{corr}) over a frequency range from 100 kHz to 10 mHz with a 10 mV peak-to-peak amplitude using the AC signal. First, the inhibition efficiency (*IE* %) is calculated starting from the charge transfer resistance, as in equation 2.

$$IE(\%) = \frac{R_{\text{ct(inh)}} - R_{\text{ct(0)}}}{R_{\text{ct(inh)}}} \times 100 \quad (2)$$

2.4. DFT computational details

Complete geometrical optimizations of the title compounds (Qui^+, Br^- and *iso*Qui^+, Br^-) were optimized employing the density functional theory (DFT) [15], including Grimme's dispersion corrected ωB97X-D3 [16] functional, and in combination with the 6-311++G(d,p) basis sets [17]. All calculations were done by using the ORCA package program (Version 4.2.1) [18], employing the SMD solvation model [19], and using water as a solvent (dielectric constant=80.4 and refractive index=1.33). The natural population analysis (NPA) was carried out by using the JANPA program (version 2.02) [20]. Molecular electronic structures and orbitals were visualized using the Avogadro software [21]. To compare the chemical reactivity of Qui^+, Br^- and *iso*Qui^+, Br^-, different quantum chemical descriptors have been calculated, such as the highest occupied molecular orbital energy (E_{HOMO}), lowest unoccupied molecular orbital energy (E_{LUMO}), energy gap (ΔE_{gap}), dipole

moment (μ), polarizabilities <α>, global hardness (η), global softness (σ), global electrophilicity (ω), the fraction of electrons transferred (Δ*N*) and back donations of electrons (Δ*E*back-d), defined by the following Equations (3) to (11) [22–24]:

$$I = -E_{\mathrm{HOMO}} \tag{3}$$

$$A = -E_{\mathrm{LUMO}} \tag{4}$$

$$\Delta E = E_{\mathrm{LUMO}} - E_{\mathrm{HOMO}} \tag{5}$$

$$< \alpha >= \frac{1}{3}(\alpha_{xx} + \alpha_{yy} + \alpha_{zz}) \tag{6}$$

$$\eta = \frac{E_{\mathrm{LUMO}} - E_{\mathrm{HOMO}}}{2} \tag{7}$$

$$\sigma = \frac{1}{\eta} \tag{8}$$

$$\omega = \frac{\chi^2}{2\eta} \tag{9}$$

$$\Delta E_{\text{back-d}} = -\frac{\eta}{4} \tag{10}$$

$$\Delta N = \frac{(\chi_{\mathrm{M}} - \chi_{\mathrm{mol}})}{2(\eta_{\mathrm{M}} + \eta_{\mathrm{mol}})} \tag{11}$$

where χ_M and χ_{mol} in equation 9 represent the metal's and the inhibitor's absolute electronegativity, respectively. According to R.G. Pearson, this study used the theoretical values χ_M=4.06 eV and η_M=0 eV for iron [25].

3. Results and Discussion

3.1. The open-circuit potentials tests

Determining the equilibrium state by measuring the open circuit potential (OCP) variation with time for the working electrode is necessary before electrochemical corrosion rate measurement. The displacement in OCP values of up to ±85 mV compared to the blank is an essential parameter that permits the classification of the inhibitor type [26, 27]. Figure 2 shows the variation of the OCP as a function of time for steel in 0.5 M H_2SO_4 in the absence and presence of various inhibitor concentrations. OCP values obtained in 0.5 M H_2SO_4 solution in the presence of both inhibitors and recorded upon reaching the steady state are positive relative to OCP values obtained in 0.5 M H_2SO_4 solution. In the blank solution, the electrode OCP value was –468 mV *vs*. ECS. The difference in the open circuit potential values for Qui^+, Br^- and *iso*Qui^+, Br^- at 5 mM is –443 and –444 mV *vs*. ECS, respectively. The resulting OCP values indicate the mixed type of both inhibitors, which will be discussed later. This result agrees well with other reported work [28].

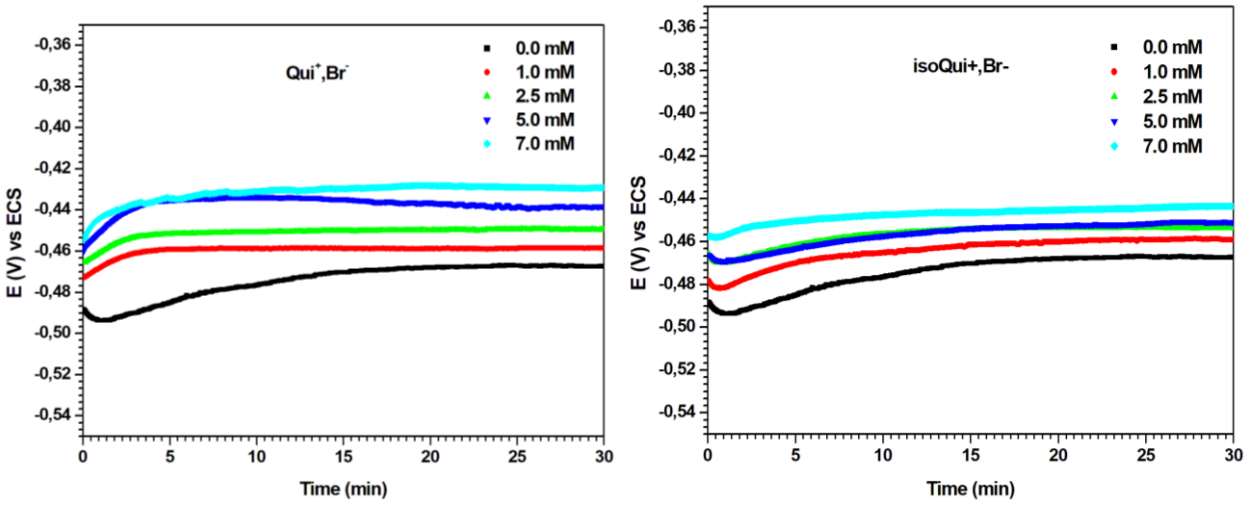

Figure 2. Open circuit potential of steel E24 immersed in 0.5 M H_2SO_4 with and without inhibitors at different concentrations.

3.2. Potentiodynamic polarization studies

The kinetics and mechanism of the anodic dissolution of steel in the sulfuric acid medium have been extensively studied. Potentiodynamic polarization measurements are generally used to obtain relevant information about electrochemical corrosion parameters [29, 30]. The Tafel plots of steel E24 in H_2SO_4 (0.5 M) at various concentrations of Qui^+, Br^- and *iso*Qui^+, Br^- are shown in Figure 3. The electrochemical dissolution of Fe can be expressed by the following mechanism [31, 32]:

$$Fe \rightarrow Fe^{2+} + 2e$$

$$2H^+ + 2e \rightarrow H_2$$

As shown in Figure 3, the Tafel slopes remain almost constant for the cathodic branches. Consequently, the corrosion kinetics occurs without changing the corrosion process mechanism controlled by activation inhibition [26, 33]. However, a significant change was observed in the anodic curves. The plateau between –0.48 V and –0.3 V is due to the formation of a film on the steel surface that becomes larger with the increase in inhibitor concentration, indicating more adsorbents on it [34].

Furthermore, the effect of inhibitors on corrosion inhibition is reflected in the offset of the anodic and cathodic curves to lower the current densities relative to the blank. It can be seen that, in the presence of both inhibitors, current density values in the cathodic branch were more affected as compared to the current density values in the anodic branch, indicating that a cathodic reaction is the most affected. In addition, the offset of the E_{corr} value is less than 85 mV. These results indicate that both inhibitors exhibit mixed-type behaviour with predominantly controlled cathodic reactions. [27, 28, 34].

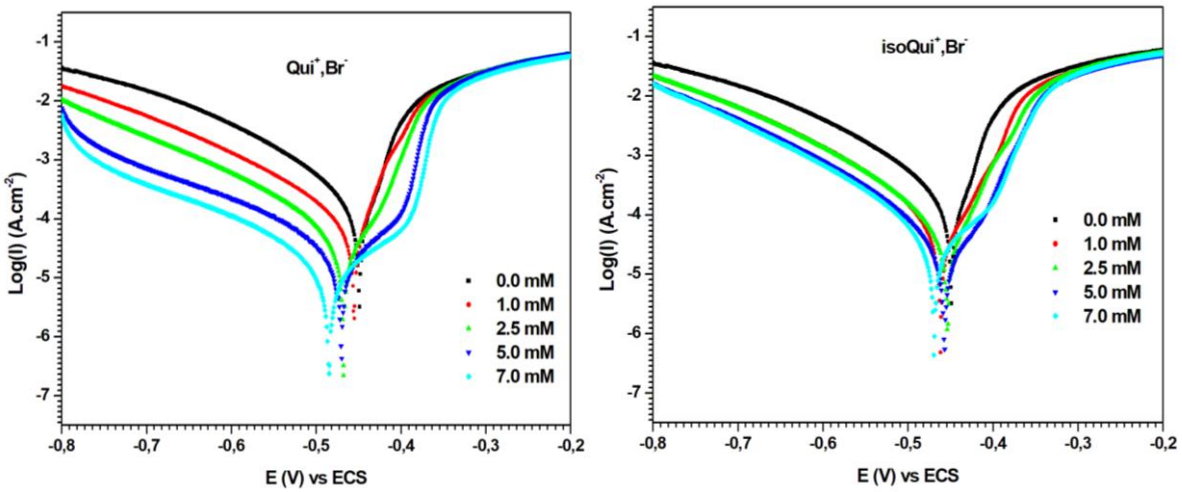

Figure 3. Potentiodynamic polarization curves were obtained for steel E24 in 0.5M H_2SO_4 without and with different concentrations of inhibitors.

The electrochemical corrosion parameters, such as corrosion currents densities (I_{corr}) and corrosion potentials (E_{corr}), have been obtained by the Tafel extrapolation method of the polarization curves, and the obtained values are listed in Table 1.

Table 1. Polarization measurements for steel E24 corrosion in the absence and presence of different inhibitor concentrations.

Inhibitor	C_{inh} **(mM)**	E_{corr} **(mV/ECS)**	I_{corr} **(μA·cm^{-2})**	***EI*** **(%)**
Blank	0	–449	384	–
Qui^+, Br^-	1	–467	301	21.61
	2.5	–457	72	81.25
	5	–462	35.8	90.68
	7	–485	30.5	92.06
isoQui^+,Br^-	1	–461	101	73.7
	2.5	–453	90.6	76.4
	5	–457	36.9	90.04
	7	–469	35.0	90.88

Table 1 shows that the efficiency inhibition increased with increasing inhibitor concentration, which was affirmed by the decrease in i_{corr} values. The studied inhibitors follow the efficiency sequence: Qui^+, $Br^- >$ *iso*Qui^+, Br^-.

3.3. Impedance measurements

To study the surface properties of steel and the mechanism of processes on the electrode, we performed electrochemical impedance measurements on E24 steel in 0.5 M H_2SO_4 solution with different concentrations of inhibitors. The results are shown in Figures 4 and 5 with the Nyquist and Bode curves for steel immersed in the corrosion solution with and without the inhibitor.

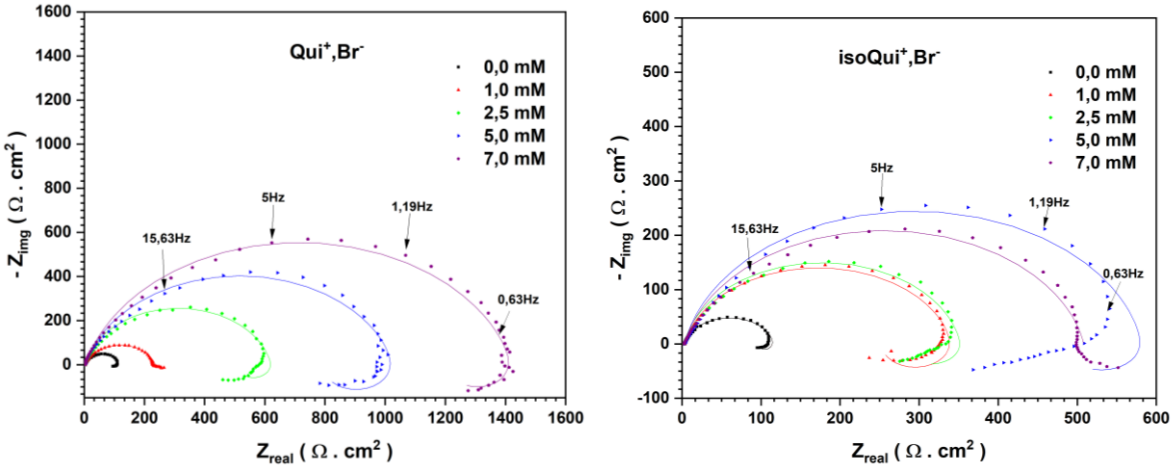

Figure 4. Nyquist plot for Steel E24 in 0.5 M H_2SO_4 with and without different concentrations of inhibitors.

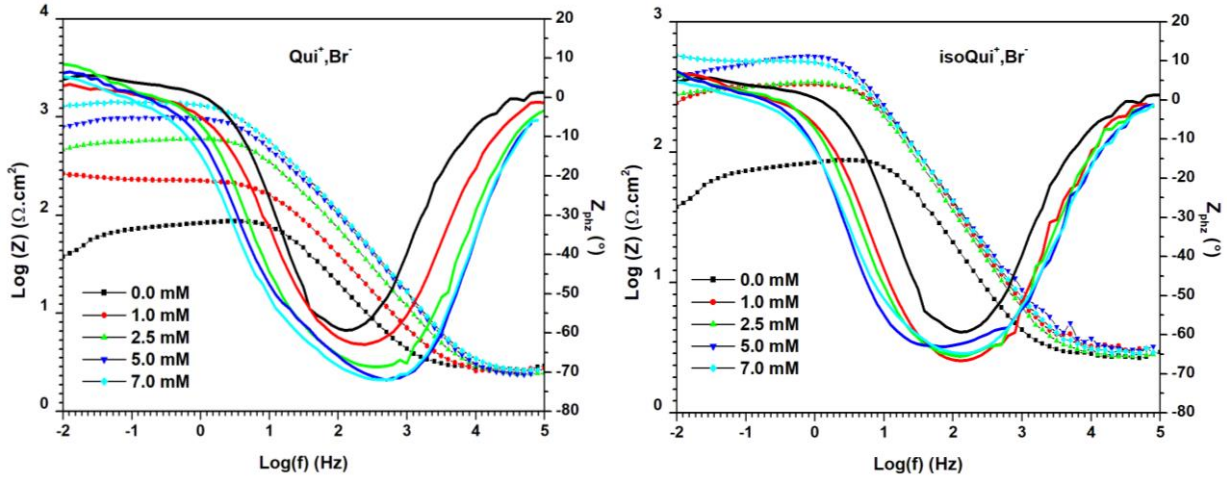

Figure 5. Bode plot for steel E24 in 0.5 M H_2SO_4 with and without different concentrations of inhibitors.

We performed electrochemical impedance spectroscopy measurements to obtain information about the double layer. As shown in Figure 4, all high-frequency loops have compressed semicircles format. It results from scattering factors due to working electrode inhomogeneity [35]. The diameters of these capacitive loops increase with the increase in the amount of inhibitor and signify an increase in the resistance (R_{ct}), *i.e.*, the charge transfer

process. Moreover, inductive loops are found in the low-frequency region that infers the adsorption and non-desorption of intermediate corrosion products and corrosion inhibitors [36–37]. The amplitude of the inductive loops increases with concentration with no difference in the shape of the curves, which means that the different steps that determine the corrosion mechanism do not change [38].

The above impedance data was analyzed using an electrochemical equivalent circuit shown in Figure 6. R_s, R_{ct}, R_L, L and CPE are the resistance solution, charge transfer resistance, resistance Indictance, inductance and constant phase element, respectively. In addition, CPE was introduced to replace a double-layer capacitance (C_{dl}) for a more accurate fit.

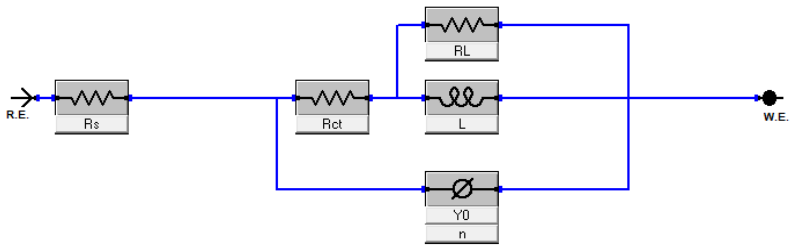

Figure 6. Equivalent circuit diagrams used to fit impedance data.

The impedance constant phase element (Z_{CPE}) is represented by [39]:

$$Z_{CPE} = \frac{1}{Y_0(j\omega)^n} \tag{12}$$

where Y_0 is a proportionality coefficient, j: imaginary unit ($j^2 = -1$), n is a *CPE* exponent with values between 0 and 1 and can be used to gauge the surface inhomogeneity, ω is the angular frequency given by $\omega = 2\pi \cdot f_{max}$. The CPE components Y_0 and n were used in the calculation of the double-layer capacitance (C_{dl}) of the adsorbed film following equation 13 [40]:

$$C_{dl} = (Y_0 \cdot R_{ct}^{1-n})^{1/n} \tag{13}$$

As shown by solid lines in Figure 4, the fitness accuracy of the equivalent circuit was checked by plotting the simulated Nyquist plots. These data indicate that when the concentration of Quinolinium bromide derivatives increases, the CPE values decrease and R_{ct} increases. The decrease in capacitance resulting from a reduction of dielectric constant and/or the increase in the electrical double layer thickness suggest that both studied compounds act by adsorption on the metal/electrolyte interface [41, 42]. In the present case, it can be assumed that Quinolinium bromide molecules replace water molecules adsorbed on the surface of the steel. The inhibition efficiency was raised to above 98% at 5 mM, confirming that the novel inhibitor has an excellent inhibition performance for steel E24 alloy in 0.5 M H_2SO_4.

The variation of Modulus and phase angle in Bode diagrams are represented in Figure 5. The modulus impedance in the low-frequency region reveals the increase in the resistance

of the adsorbent film as the concentration increases [38]. In the phase angle, only a one-time constant indicates that the charge transfer process mainly controls the dissolution of steel in an acidic solution [43].

Table 2. Impedance parameters for steel E24 in 0.5 M H_2SO_4 solution in the absence and presence of different inhibitor concentrations.

Inhibitor	C_{inh} (mM)	R_s ($\Omega \cdot cm^2$)	R_{ct} ($\Omega \cdot cm^2$)	n	$Y_0\ 10^{-6}$ ($S^n \cdot cm^2 \cdot \Omega^{-1}$)	C_{dl} ($\mu F \cdot cm^{-2}$)	R_L ($\Omega \cdot cm^2$)	L (*H*)	*IE* (%)
Blank	0	3.656	90.0	0.8956	140.0	84.1	23	20	
Qui^+, Br^-	1	2.424	233.6	0.8317	115.0	55.3	–	–	61.34
	2.5	2.347	500.0	0.8784	44.59	26.3	120	1400	82.00
	5	2.094	790.0	0.8450	43.43	23.4	240	1500	88.61
	7	2.354	1205	0.8415	41.62	23.7	222.8	2285	92.53
isoQui^+, Br^-	1	3.109	249.5	0.8789	83.77	49.2	90	350	63.93
	2.5	2.784	275.0	0.9008	80.60	53.0	75	1200	67.27
	5	3.249	480.0	0.8917	70.0	46.4	100	1200	81.25
	7	2.935	505.0	0.8770	80.90	51.7	–	–	82.17

3.4. Adsorption isotherm simulation

In this work, to further investigate the adsorption process, we have evaluated the composition of several typical adsorption isotherms (Temkin, Frumkin, Langmuir isotherms). Langmuir isotherm was the best description of the adsorption behaviour after calculating the correlation coefficient values (R^2). The corresponding formula is followed [44].

$$\frac{C_{inh}}{\theta} = \frac{1}{K} + C_{inh} \tag{14}$$

θ is the surface coverage, and K_{ads} represents the adsorption equilibrium constant. The standard free energy of adsorption (ΔG^{o}_{ads}) can be deduced from Equation 15 [44]:

$$K_{ads} = \frac{1}{55.5} \exp\left(\frac{-\Delta G^0_{ads}}{RT}\right) \tag{15}$$

Herein, we have calculated K_{ads} from the straight lines of Langmuir from Figure 7. The values of ΔG^0_{ads} can be obtained from the equation above. The adsorption model was classified as physisorption when the absolute value of ΔG^0_{ads} is lower than 20 kJ/mol, while

the inhibitors act by chemisorption model when the ΔG^0_{ads} is greater than 40 kJ/mol value [34]. The calculated ΔG^0_{ads} values are –29.08 and –30.41 kJ/mol for Qui^+, Br^- and *iso*Qui^+, Br^-, respectively. This calculation shows that the adsorption of quinolinium bromide derivatives on steel is chemical and physical.

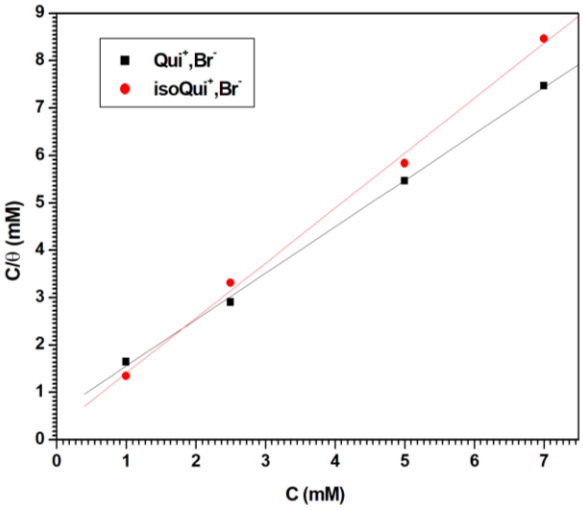

Figure 7. Langmuir adsorption for steel E24 in 0,5 M H_2SO_4 with different concentrations of inhibitors at 25°C.

3.5. Theoretical results

The optimized geometry structures of the title compounds with their selected bond lengths are presented in Figure 8. In addition, all values of the bond lengths, bond angles, and dihedral angles are reported in supplementary Tables S1–S3.

According to the optimized structures (Figure 8), we can find that the bromide (Br^-) ion can form non-covalent interactions with Qui^+ and *iso*Qui^+, respectively. Similar behaviour is observed in both Qui^+, Br^- and *iso*Qui^+, Br^- complexes, in which the bromide (Br^-) ion interacts with the hydrogen atoms of both the aromatic ring and also the substituent group (2-methoxy-2-oxoethyl) of Qui^+ and *iso*Qui^+ compounds, respectively, with distances in the range of 2.533–2.801 Å, as shown in Figure 8. However, in the *iso*Qui^+ compounds, we should also note that the bromide (Br^-) ion lies practically in the same plane as the aromatic ring. On the contrary, for the Qui^+ compound, the bromide (Br^-) ion is not positioned in the same plane as the aromatic ring (see Figure 8).

To explore and optimize the non-covalent forces between the bromide (Br^-) ion and organic molecular fragments (Qui^+ and *iso*Qui^+) that appear to be involved in the stability of both complexes Qui^+, Br^- and *iso*Qui^+, Br^-, the reduced density gradient (RDG) analysis is employed [45, 46].

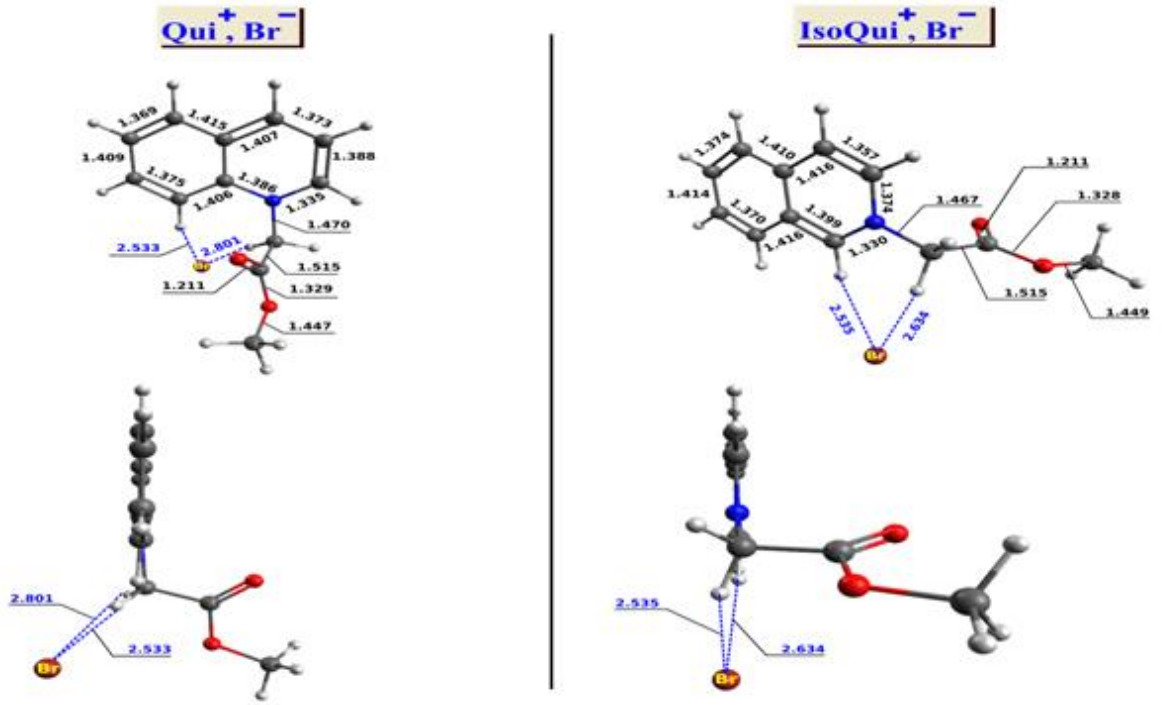

Figure 8. The optimized geometry structures of the title compounds: Qui^+, Br^- (left) and *iso*Qui^+, Br^- (right).

Figure 9 shows the RDG plots (RDG-scatter plot (top) and RDG-isosurface (bottom)), in which the blue, green, and red regions represent the strong, attractive interactions like H-bond, van der Waals interactions, and strong steric effects, respectively.

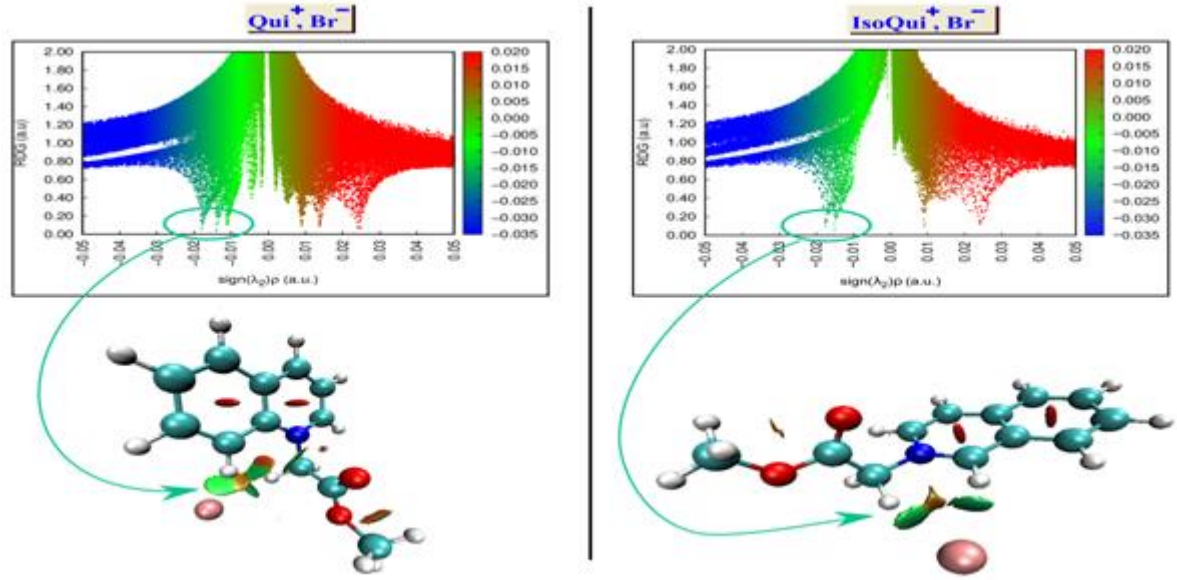

Figure 9. The NCI-RDG isosurfaces (bottom) and scatter plot (top) of the title compounds; Qui^+, Br^- (left) and *iso*Qui^+, Br^- (right).

NCI-RDG analysis reveals a green isosurface between the bromide (Br^-) ion and hydrogen atoms of both the Qui^+ and *iso*Qui^+, indicating that the vdW interaction is the key driving force for the interaction between Br^- and organic molecular fragments (Qui^+ and *iso*Qui^+).

Frontier molecular orbitals (HOMO and LUMO) of both Qui^+, Br^- and *iso*Qui^+, Br^- complexes are shown in Figure 10. Analysis of these results indicates that the HOMO density is mainly localized at the bromide (Br^-) ion for both Qui^+, Br^- and *iso*Qui^+, Br^-, suggesting the most reactivity centres for bonding to surface through donating electrons to the mild steel surface. At the same time, the LUMO density distribution indicates that the aromatic ring for both Qui^+, Br^- and *iso*Qui^+, Br^- complexes are the centres with the highest tendency to accept electrons from the d-orbital of the metal.

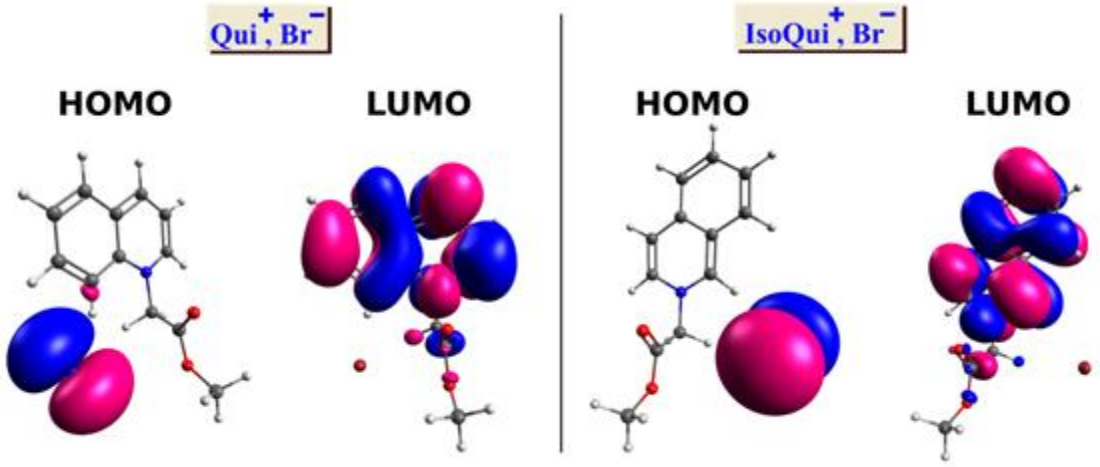

Figure 10. Frontier molecular orbitals (HOMO and LUMO) of the title compounds; Qui^+, Br^- (left) and *iso*Qui^+, Br^- (right).

Table 3. Calculated the title compounds' quantum chemical descriptors (a) at ωB97X-D3/6-311++G (d, p) level theory.

Descriptor	**Qui^+, Br^-**	***iso*Qui^+, Br^-**
E_{HOMO} (eV)	–7.96	–8.09
E_{LUMO}(eV)	–0.86	–0.63
ΔE_{gap}(eV)	7.10	7.46
I (eV)	7.96	8.09
A (eV)	0.86	0.63
μ (Debye)	19.64	18.38
<α> (a.u.)	257.66	258.69
V^{vdw} (Bohr^3)	2168.52	2134.77

Descriptor	**Qui$^+$, Br$^-$**	***iso*Qui$^+$, Br$^-$**
SA (Bohr^2)	1054.18	1029.12
TE (a.u.)	–3243.91	–3243.91
χ	4.41	4.36
π	–4.41	–4.36
η	3.55	3.73
σ	0.28	0.27
ω	2.74	2.55
Δ*N*	–0.049	–0.039
$\Delta n_{\text{back-d}}$	–0.89	–0.93

[(a)]: Energy gap (ΔE_{gap}); Electron affinity (*A*); Ionization potential (*I*); Dipole moment (μ); Total energy (*TE*); Electronegativity (χ); Polarizability <α>; Chemical potential (π); Global softness (σ); Global hardness (η); Global Electrophilicity (ω); Fraction of electrons transferred (Δ*N*) and back-donation (Δ*E*back-d).

The results of quantum-calculated global descriptors for title compounds Qui$^+$, Br$^-$ and *iso*Qui$^+$, Br$^-$ are listed in Table 3. In literature, it has been reported that the molecule with a low LUMO-HOMO energy gap (ΔE_{gap}) is probably associated with high chemical reactivity, and vice versa; the existence of a large HOMO-LUMO gap is generally associated with low chemical reactivity [22–23].

From the results of Table 3, the Qui$^+$, Br$^-$ compound has the lowest value of ΔE_{gap}, which means the highest reactivity than of the compound *iso*Qui$^+$, Br$^-$. This result agrees with our previous experimental observations, suggesting that the compound Qui$^+$, Br$^-$ has the highest inhibition efficiency. The results obtained reveal that the Qui$^+$, Br$^-$ has higher electronegativity (χ), global softness (σ), and global electrophilicity (ω) than the *iso*Qui$^+$, Br$^-$ compound. However, according to the DFT calculations (Table 3), the Qui$^+$, Br$^-$ and *iso*Qui$^+$, Br$^-$ provided an almost similar behaviour due to the very close values.

Conclusion

1. The corrosion inhibition efficiency of 2-methoxy-2-oxoethyl)quinolinium bromide (Qui$^+$, Br$^-$) and (2-methoxy-2-oxoethyl) iso quinolinium bromide (*iso*Qui$^+$, Br$^-$) were studied.
2. Corrosion inhibition efficiencies increase as the concentration of inhibitors increases, exceeding 90% for both inhibitors.
3. Potentiostatic polarization revealed that both inhibitors affected cathodic and anodic reactions, making them inhibitors of a mixed type.
4. The compounds' adsorption showed chemical and physical interactions between the molecules and the metal and was found to fit the Langmuir adsorption isotherm.

5. The study demonstrates that quinolinium molecules could serve as corrosion inhibitors for steel due to their kinetic control and strong adsorption on the surface.
6. Results obtained from all the experimental methods agree with the theoretical study.

Acknowledgments

We thank MESRS (Ministère de l'Enseignement Supérieur et de la Recherche Scientifique) Algeria, for Financial support.

References

1. I.A. Zaafarany, Corrosion Inhibition of Mild Steel in Hydrochloric Acid Solution using Cationic Surfactant Olyel-amido Derivatives, *Int. J. Electrochem. Sci*., 2013, **8**, no. 7, 9531–9542.
2. A.S. Yaro, A.A. Khadom and R.K. Wael, Apricot juice as green corrosion inhibitor of mild steel in phosphoric acid, *Alexandria. Eng. J*., 2013, **52**, no. 1, 129–135. doi: 10.1016/j.aej.2012.11.001
3. L. Zhu, C. Yang, D. Long and Z. Chen, Corrosion failure analysis of 20# steel in the process of natural gas purification, *Russ. J. Appl. Chem*., 2015, **88**, no. 9, 1510–1516. doi: 10.1134/S1070427215090207
4. Y. He, Q. Yang and Z. Xu, A supramolecular polymer containing β-cyclodextrin as corrosion inhibitor for carbon steel in acidic medium, *Russ. J. Appl. Chem*., 2014, **87**, no. 12, 1936–1942. doi: 10.1134/S1070427214120234
5. Z. Moallem, I. Danaee and H. Eskandari, Corrosion Inhibition and Adsorption Behavior of Gentian Violet on AISI 4130 Alloy Steel in HCl Solution, *Trans. Indian Inst. Met*., 2014, **67**, no. 6, 817–825. doi: 10.1007/s12666-014-0403-x
6. Y. He, Y. Zhou, R. Yang, L. MA and Z. Chen, Imidazoline derivative with four imidazole reaction centers as an efficient corrosion inhibitor for anti-CO_2 corrosion, *Russ. J. Appl. Chem*., 2015, **88**, no. 7, 1192–1200. doi: 10.1134/S1070427215070149
7. X. Liu, Y. Lu, Y.S. Yang, H.X. Hu and Y.G. Zheng, Electrochemical behavior of phenylalanine and its cobalt complex as corrosion inhibitors for mild steel in H_2SO_4, *Russ. J. Appl. Chem*., 2015, **88**, no. 2, 350–355. doi: 10.1134/S1070427215020263
8. H. Elmsellem, M.H. Youssouf, A. Aouniti, T. Ben Hadda, A. Chetouani and B. Hammouti, Adsorption and inhibition effect of curcumin on mild steel corrosion in hydrochloric acid, *Russ. J. Appl. Chem*., 2014, **87**, no. 6, 744–753. doi: 10.1134/S1070427214060147
9. X. Liu, H. Cao and B. Jiang, The inhibitory effect of bipyridine and its cobalt complex on the corrosion behaviour of carbon steel in acidic medium, *Russ. J. Appl. Chem*., 2014, **87**, no. 6, 738–743. doi: 10.1134/S1070427214060135
10. T.I. Gorbunova, D.N. Bazhin, A.Y. Zapevalov and V.I. Saloutin, Inhibitory activity of fluorine-containing quaternary ammonium salts comprising an N-methyl piperazinyl moiety, *Russ. J. Appl. Chem*., 2013, **86**, no. 7, 992–996. doi: 10.1134/S1070427213070082

11. S.M. Elhadi, M. Bilel, B. Abdelmalek and C. Aissa, Experimental evaluation of quinolinium and isoquinolinium derivatives as corrosion inhibitors of mild steel in 0.5 M H_2SO_4 solution, *Prot. Met. Phys. Chem. Surf.*, 2016, **52**, no. 4, 731–736. doi: 10.1134/S2070205116040092
12. F. El-Hajjaji, M. Messali, M.V. Martínez de Yuso, E. Rodríguez-Castellón, S. Almutairi, T.J. Bandosz and M. Algarra, Effect of 1-(3-phenoxypropyl) pyridazin-1-ium bromide on steel corrosion inhibition in acidic medium, *J. Colloid Interface Sci*., 2019, **541**, 418–424. doi: 10.1016/j.jcis.2019.01.113
13. A. Choi, R.M. Morley and I. Coldham, Synthesis of pyrrolo[1,2-*a*]quinolines by formal 1,3-dipolar cycloaddition reactions of quinolinium salts, *Beilstein J. Org. Chem*., 2019, **15**, 1480–1484. doi: 10.3762/bjoc.15.149
14. J. Brioche, C. Meyer and J. Cossy, Synthesis of 2-Aminoindolizines by 1,3-Dipolar Cycloaddition of Pyridinium Ylides with Electron-Deficient Ynamides, *Org. Lett*., 2015, **17**, no. 11, 2800–2803. doi: 10.1021/acs.orglett.5b01205
15. P. Geerlings, F. De Proft and W. Langenaeker, Conceptual Density Functional Theory, *Chem. Rev*., 2003, **103**, no. 5, 1793–1874. doi: 10.1021/cr990029p
16. Y.-S. Lin, .G.-D. Li, S.-P. Mao and J.-D.Chai, Long-Range Corrected Hybrid Density Functionals with Improved Dispersion Corrections, *J Chem. Theory Comput.* 2013, **9**, no. 1, 263–272. doi: 10.1021/ct300715s
17. W.J. Hehre, Ab initio molecular orbital theory, *Acc. Chem. Res*., 1976, **9**, no. 11, 399–406. doi: 10.1021/ar50107a003
18. F. Neese, The ORCA program system, *Wiley Interdiscip. Rev.: Comput. Mol. Sci*., 2012, **2**, no. 1, 73–78. doi: 10.1002/wcms.81
19. A.V. Marenich, C.J. Cramer and D.G. Truhlar, Performance of SM6, SM8, and SMD on the SAMPL1 Test Set for the Prediction of Small-Molecule Solvation Free Energies, *J. Phys. Chem. B*., 2009, **113**, no. 14, 4538–4543. doi: 10.1021/jp809094y
20. T.Y. Nikolaienko, L.A. Bulavin and D.M. Hovorun, JANPA: An open source cross-platform implementation of the Natural Population Analysis on the Java platform, *Comput. Theor. Chem*., 2014, **1050**, 15–22. doi: 10.1016/j.comptc.2014.10.002
21. M.D. Hanwell, D.E. Curtis, D.C. Lonie, T. Vandermeersch, E. Zurek and G.R. Hutchison, Avogadro: an advanced semantic chemical editor, visualization, and analysis platform, *J. Cheminf*., 2012, **4**, no. 1, 17. doi: 10.1186/1758-2946-4-17
22. S. Peljhan and A. Kokalj, Adsorption of Chlorine on Cu(111): A Density-Functional Theory Study, *J. Phys. Chem. C*., 2011, **113**, no. 32, 14363–14376. doi: 10.1021/jp902273k
23. H. Allal, Y. Belhocine and E. Zouaoui, Computational study of some thiophene derivatives as aluminium corrosion inhibitors, *J. Mol. Liq*., 2018, **265**, 668–678. doi: 10.1016/j.molliq.2018.05.099
24. I.B. Obot, I.B. Onyeachu and S.A. Umoren, Pyrazines as Potential Corrosion Inhibitors for Industrial Metals and Alloys: A Review, *J. Bio- Tribo-Corros*., 2018, **4**, no. 2, 18. doi: 10.1007/s40735-018-0135-2

25. R.G. Pearson, The HSAB Principle – more quantitative aspects, *Inorg. Chim. Acta*., 1995, **240**, no. 1–2, 93–98. doi: 10.1016/0020-1693(95)04648-8
26. M.M. Solomon, S.A. Umoren, M.A. Quraishi and M. Salman, Myristic acid based imidazoline derivative as effective corrosion inhibitor for steel in 15% HCl medium, *J. Colloid Interface Sci*., 2019, **551**, 47–60. doi: 10.1016/j.jcis.2019.05.004
27. M.M. Solomon and S.A. Umoren, In-situ preparation, characterization and anticorrosion property of polypropylene glycol/silver nanoparticles composite for mild steel corrosion in acid solution, *J. Colloid Interface Sci*., 2016, **462**, 29–41. doi: 10.1016/j.jcis.2015.09.057
28. H. Gerengi, H.I. Ugras, M.M. Solomon, S.A. Umoren, M. Kurtay and N. Atar, Synergistic corrosion inhibition effect of 1-ethyl-1-methylpyrrolidinium tetrafluoroborate and iodide ions for low carbon steel in HCl solution, *J. Adhes. Sci. Technol*., 2016, **30**, 2383–2403. doi: 10.1080/01694243.2016.1183407
29. G. Kear, B.D. Barker and FC. Walsh, Electrochemical corrosion of unalloyed copper in chloride media—a critical review, *Corros. Sci*., 2004, **46**, no. 1, 109–135. doi: 10.1016/S0010-938X(02)00257-3
30. D. Zhang, L. Gao and G. Zhou, Inhibition of copper corrosion by bis-(1-benzotriazolymethylene)-(2,5-thiadiazoly)-disulfide in chloride media, *Appl. Surf. Sci*., 2004, **225**, no. 1–4, 287–293. doi: 10.1016/j.apsusc.2003.10.016
31. K.F. Khaled, M.N. Hamed, K.M. Abdel-Azim and N.S. Abdelshafi, Inhibition of copper corrosion in 3.5% NaCl solutions by a new pyrimidine derivative: electrochemical and computer simulation techniques, *J. Solid State Electrochem*., 2011, **15**, no. 4, 663–673. doi: 10.1007/s10008-010-1110-0
32. M.M. Antonijević, S.M. Milić and M.B. Petrović, Films formed on copper surface in chloride media in the presence of azoles, *Corros. Sci*., 2009, **51**, no. 6, 1228–1237. doi: 10.1016/j.corsci.2009.03.026
33. N. Kumari, P.K. Paul, L. Gope and M. Yadav, Studies on anticorrosive action of synthesized indolines on mild steel in 15% HCl solution, *J. Adhes. Sci. Technol*., 2016, **31**, no. 14, 1524–1544. doi: 10.1080/01694243.2016.1263473
34. Y. Xu, S. Zhang, W. Li, L. Guo, S. Xu, L. Feng and L.H. Madkour, Experimental and theoretical investigations of some pyrazolo-pyrimidine derivatives as corrosion inhibitors on copper in sulfuric acid solution, *Appl. Surf. Sci*., 2018, **459**, 612–620. doi: 10.1016/j.apsusc.2020.146451
35. M. Lebrini, M. Lagrenee, H. Vezin, M. Traisnel and F. Bentiss, Experimental and theoretical study for corrosion inhibition of mild steel in normal hydrochloric acid solution by some new macrocyclic polyether compounds, *Corros. Sci*., 2007, **49**, no. 5, 2254–2269. doi: 10.1016/j.corsci.2006.10.029
36. S.S. Abd El Rehim, H.H. Hassan and M.A. Amin, Corrosion inhibition study of pure Al and some of its alloys in 1.0 M HCl solution by impedance technique, *Corros. Sci*., 2004, **46**, no. 1, 5–25. doi: 10.1016/S0010-938X(03)00133-1

37. M. Kissi, M. Bouklah, B. Hammouti and M. Benkaddour, Establishment of equivalent circuits from electrochemical impedance spectroscopy study of corrosion inhibition of steel by pyrazine in sulphuric acidic solution, *Appl. Surf. Sci*., 2006, **252**, no. 12, 4190–4197. doi: 10.1016/j.apsusc.2005.06.035
38. T. Zhang, W. Jiang, H. Wang, and S. Zhang, Synthesis and localized inhibition behaviour of new triazine-methionine corrosion inhibitor in 1 M HCl for 2024-T3 aluminium alloy, *Mater. Chem. Phys*., 2019, **237**, 121866. doi: 10.1016/j.matchemphys.2019.121866
39. M. Das, A. Biswas, B.K. Kundu, S.M. Mobin, G. Udayabhanu and S. Mukhopadhyay, Targeted synthesis of cadmium (II) Schiff base complexes towards corrosion inhibition on mild steel, *RSC Adv*., 2017, **7**, no. 77, 48569–48585. doi: 10.1039/C7RA08633D
40. N. El Hamdani, R. Fdil, M. Tourabi, C. Jama and F. Bentiss, Alkaloids extract of *Retama monosperma (L.) Boiss.* seeds used as a novel eco-friendly inhibitor for carbon steel corrosion in 1 M HCl solution: Electrochemical and surface studies, *Appl. Surf. Sci*., 2015, **357**, 1294–1305. doi: 10.1016/j.apsusc.2015.09.159
41. D.S. Chauhan, K. Ansari, A.A. Sorour, M.A. Quraishi, H. Lgaz and R. Salghi, Thiosemicarbazide and thiocarbohydrazide functionalized chitosan as ecofriendly corrosion inhibitors for carbon steel in hydrochloric acid solution, *Int. J. Biol. Macromol*., 2018, **107**, 1747–1757. doi: 10.1016/j.ijbiomac.2017.10.050
42. P. Singh, E.E. Ebenso, L.O. Olasunkanmi, I.B. Obot and M.A. Quraishi, Electrochemical, Theoretical, and Surface Morphological Studies of Corrosion Inhibition Effect of Green Naphthyridine Derivatives on Mild Steel in Hydrochloric Acid, *J. Phys. Chem. C*., 2016, **120**, no. 6, 3408–3419. doi: 10.1021/acs.jpcc.5b11901
43. M. Hrimla, L. Bahsis, A. Boutouil, M. Laamari, M. Julve and S.-E. Stiriba, A combined computational and experimental study on the mild steel corrosion inhibition in hydrochloric acid by new multifunctional phosphonic acid containing 1,2,3-triazoles, *J. Adhes. Sci. Technol*., 2020, **34**, no. 16, 1741–1773. doi: 10.1080/01694243.2020.1728177
44. A.E. Vazquez, L.A.L. Reséndiz, I.A. Figueroa, F.J.R. Gómez, M. Figueroa, D.Á. Beltrán, M. Castro and A. Miralrio, Corrosion inhibition assessment on API 5L X70 steel by preussomerin G immersed in saline and saline acetic, *J. Adhes. Sci. Technol*., 2021, **35**, no. 8, 873–899. doi: 10.1080/01694243.2020.1826828
45. N. Ammouchi, H. Allal, E. Zouaoui, K. Dob, D. Zouied and M. Bououdina, Extracts of Ruta Chalepensis as Green Corrosion Inhibitor for Copper CDA 110 in 3% NaCl Medium: Experimental and Theoretical Studies, *Anal. Bioanal. Electrochem*., 2019, **11**, no. 7, 830–850.
46. A. Otero-de-la-Roza and E.R. Johnson, A benchmark for non-covalent interactions in solids, *J. Phys. Chem*., 2012, **137**, 054103. doi: 10.1063/1.4738961

♦ ♦ ♦